energies

MDPI

Article

Hydrodynamic Investigation of an Oscillating Buoy Wave Energy Converter Integrated into a Pile-Restrained Floating Breakwater

Xuanlie Zhao, Dezhi Ning *, Chongwei Zhang and Haigui Kang

State Key Laboratory of Coastal and Offshore Engineering, Dalian University of Technology, Dalian 116024, China; zhaoxuanlie@163.com (X.Z.); chongweizhang@dlut.edu.cn (C.Z.); hgkang@dlut.edu.cn (H.K.)

* Correspondence: dzning@dlut.edu.cn; Tel.: +86-411-8470-8267

Academic Editor: Frede Blaabjerg

Received: 27 March 2017; Accepted: 10 May 2017; Published: 18 May 2017

Abstract: An analytical model is developed based on linear potential flow theory and matching eigenfunction expansion technique to investigate the hydrodynamics of a two-dimensional floating structure. This structure is an integration system consisting of a breakwater and an oscillating buoy wave energy converter (WEC). It is constrained to heave motion, and linear power take-off (PTO) damping is used to calculate the absorbed power. The proposed model is verified against the published results. The proposed integrated structure is compared with the fixed structure and free heave-motion structure, respectively. The hydrodynamic properties of the integrated structure with the optimal PTO damping i.e., the transmission coefficient, reflection coefficient, capture width ratio (CWR), and heave response amplitude operator (RAO), are investigated. The effect of the PTO damping on the performance of the integrated system is also evaluated. Results indicate that with the proper adjustment of the PTO damping, the proposed integrated system can produce power efficiently. Meanwhile, the function of coastal protection can be compared with that of the fixed structure.

Keywords: analytical study; linear potential flow theory; floating breakwater; wave energy extraction

1. Introduction

As environmental concerns gain importance, more studies are being conducted on energy extraction from renewable energy resources. Ocean wave energy is a huge, largely untapped renewable energy resource, with the potential to attract researchers and engineers [1]. To date, a wide range of wave energy converters (WECs) has been developed [2]. However, the high construction cost still significantly impedes the industrial application of wave energy utilization [3]. Thus, an increasing number of developers have focused on reducing construction costs. Meanwhile, the greenness of the seaport has accordingly drawn considerable attention. Renewable energy utilization is regarded as one of the representative factors in evaluating the greenness of a seaport [4,5]. Combining the wave energy converter with the existing breakwater structures can simultaneously achieve wave energy utilization and wave attenuation. Cost-sharing between them can naturally lead to cost reduction. The benefits obtained from the integration of breakwaters and WECs over the isolated WECs can be seen in Mustapa et al. [6].

The breakwater–WEC integration includes two categories: fixed bottom-mounted structures and floating structures. Integrated systems, such as overtopping [7,8], oscillating water column-type (OWC type) [9,10] and piston-type WEC-breakwater integration [11], belong to the former category (for detailed descriptions see [6]). It is well understood that the floating breakwaters are favorable for their relatively low costs [12]. Recently, many attempts associated with integrations of WECs and

floating breakwaters (including truncated surface-piecing breakwaters) have been made. He et al. [13] integrated OWC-type devices into slack-moored floating breakwaters with pneumatic chambers. Experimental results showed that functions of coastal protection and the wave energy utilization can be satisfied simultaneously for the proposed concept. Mendoza et al. [14] investigated the shore protection function provided by WEC farms and found that the multi-purpose use of WECs can be achieved. Chen et al. [15] numerically investigated the hydrodynamic performance of floating horizontal cylinders as both WECs and floating breakwaters; results indicated that a configuration with small cylinders in groups may achieve the two functions simultaneously. Martinelli et al. [16] experimentally investigated the performance of a hybrid structure consisting of an "active" floating breakwater and a WEC (named ShoWED); results showed that the hybrid structure can successfully generate both electrical energy and coastal protection. Ning et al. [17] proposed a novel integrated system of a vertical pile-restrained floating breakwater that operates under the principle of an oscillating buoy WEC. The integrated system has a simple structural configuration. The experimental study showed that acceptable wave attenuation performance and energy-conversion efficiency can be obtained if the appropriate structure dimensions and power take-off (PTO) damping force are obtained. It is understood that the floating breakwaters are often used in areas characterized by low wave energy. Thus, the high performance of the device in energy conversion can determine the engineering interest.

Prompted by [17], the current study aims at theoretically revealing the relationship among the reflection coefficient, transmission coefficient, and capture width ratio (CWR) of the WEC-type breakwater. The hydrodynamics of the integrated system with the optimal PTO damping, fixed breakwater, and free heave-motion breakwater are also compared. In addition, the effect of the PTO damping on the hydrodynamic performance of the integrated device is evaluated. The present study is conducted based on potential flow theory and the assumption of breakwater undergoing heave motion with small response amplitude. The matching eigenfunction expansion method is used to solve diffraction and radiation problems. The exciting force and hydrodynamic coefficients in heave mode are computed based on [18]. The reflection coefficient K_r, transmission coefficient K_t, response amplitude operator (RAO) ξ in heave mode, and CWR η can then be derived. Note that the equation of ${K_r}^2 + {K_t}^2 + \eta = 1$ is satisfied based on the rule of energy conservation.

This study is organized as follows: Section 2 describes the formulas. Section 3 gives the dimensional analysis. Section 4 presents the validation, results, and discussions. Section 5 provides the conclusions.

2. Formulas

As shown in Figure 1, a pontoon-type structure (i.e., breakwater) with a width of $B = 2a$ and a draft d_1 is situated in the water with a uniform depth h_1. Similar to the description in [18], a 2-dimensional Cartesian coordinate (o-xz) system is employed, and the center of origin is located at the cross-point of the still water plane and medial axis of the breakwater. Correspondingly, the mass term and stiffness term of the breakwater in heave mode can be expressed as M (=$2\rho a d_1$) and K (=$2\rho g a$), where ρ denotes the density of water, and g represents the gravitational acceleration. The structure is subjected to a train of regular waves traveling in the positive x-direction. A is the incident wave amplitude, which is the maximum distance of a water particle from its equilibrium position during a period, and L is the wavelength, which is the distance that the wave travels during a wave period. The structure is assumed to respond only in heave mode.

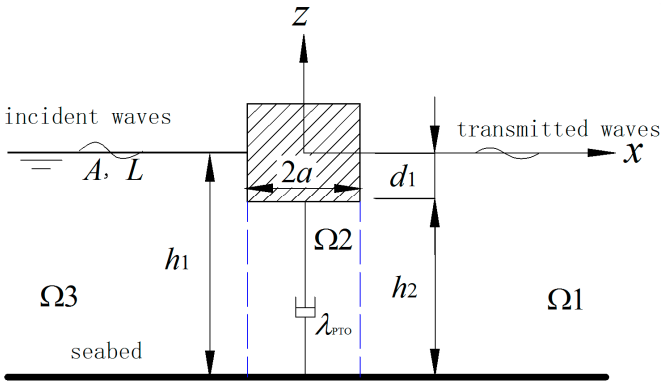

Figure 1. Sketch of the floating structure with the power take-off (PTO) system (the structure restrained with the vertical pile moves in heave and the PTO system is used to capture wave energy, detailed description see [17]).

As indicated in Figure 1, the fluid domain is divided into three subdomains—i.e., Ω_1, Ω_2, and Ω_3. The fluid motion in the whole domain can be described by the velocity potential:

$$\phi(x,z,t) = \mathrm{Re}\left[\Phi(x,z)e^{-\mathrm{i}\omega t}\right] \tag{1}$$

where t denotes time, $\mathrm{i} = \sqrt{-1}$, ω represents the angular frequency, Re [ ] denotes the real part of a complex expression and Φ is a complex spatial velocity potential, which satisfies Laplace's equation:

$$\frac{\partial^2\Phi}{\partial x^2} + \frac{\partial^2\Phi}{\partial z^2} = 0 \tag{2}$$

With heave motion being the only concern, the velocity potential Φ can be expressed as:

$$\Phi = \Phi_\mathrm{I} + \Phi_\mathrm{D} + \Phi_\mathrm{R} \tag{3}$$

where Φ_I is the incident velocity potential, Φ_D denotes the diffraction potential, and Φ_R represents the radiation potential due to heave motion.

The spatial velocity potential for the incident waves can be written as:

$$\Phi_\mathrm{I} = -\frac{\mathrm{i}gA}{\omega}\frac{\cosh[k(z+h_1)]}{\cosh(kh_1)}e^{ikx} \tag{4}$$

where k is the wavenumber, which satisfies the dispersion relation $\omega^2 = gk\tanh(kh_1)$. Correspondingly, the wavelength $L = 2\pi/k$.

For the wave diffraction problem, the governing equation is Laplace's equation, and its boundary conditions for the diffracted spatial potential can be written as follows:

$$\frac{\partial\Phi_\mathrm{D}}{\partial z} - \frac{\omega^2}{g}\Phi_\mathrm{D} = 0 \quad (z = 0, \quad x > |a|) \tag{5}$$

$$\frac{\partial\Phi_\mathrm{D}}{\partial z} = 0 \quad (z = -h_1) \tag{6}$$

$$\frac{\partial\Phi_\mathrm{D}}{\partial z} = -\frac{\partial\Phi_\mathrm{I}}{\partial z} \quad (z = -d_1,\ |x| \le a) \tag{7}$$

$$\frac{\partial\Phi_\mathrm{D}}{\partial x} = -\frac{\partial\Phi_\mathrm{I}}{\partial x} \quad (-d_1 < z < 0,\ x = \pm a) \tag{8}$$

$$\Phi_\mathrm{D}\text{outgoing;} \quad \text{finite value,} \quad |x| \to \infty \tag{9}$$

For the radiation problem, the body is forced to heave with the amplitude A_R and the angular frequency ω; thus, the radiation potential Φ_R can be written as:

$$\Phi_R = -i\omega A_R \varphi_R(x,z) \tag{10}$$

For the complex spatial velocity potential φ_R, the governing equation is Laplace equation, and its boundary conditions can be written as follows:

$$\frac{\partial \varphi_R}{\partial z} - \frac{\omega^2}{g}\varphi_R = 0 \quad (z = 0, \quad x > |a|) \tag{11}$$

$$\frac{\partial \varphi_R}{\partial z} = 0 \quad (z = -h_1) \tag{12}$$

$$\frac{\partial \varphi_R}{\partial z} = 1 \quad (z = -d_1, |x| \le a) \tag{13}$$

$$\frac{\partial \varphi_R}{\partial x} = 0 \quad (-d_1 < z < 0, x = \pm a) \tag{14}$$

$$\varphi_R \quad \text{outgoing;} \quad \text{finite value,} \quad |x| \to \infty \tag{15}$$

The frequency-dependent expressions of the diffraction potential and the radiation potential can be obtained from [18]. The vertical exciting force F_z, added mass μ, and radiation damping coefficient λ in heave mode can then be computed using the following expressions, respectively:

$$F_z = \rho i\omega \int_{S_0} (\Phi_I + \Phi_D) ds \tag{16}$$

$$\mu = \rho \int_{S_0} \mathrm{Re}[\varphi_R] n_z ds \tag{17}$$

$$\lambda = \rho \int_{S_0} \mathrm{Im}[\varphi_R] n_z ds \tag{18}$$

where S_0 is the bottom area of the structure, Re and Im denote the real and imaginary parts of a complex number, and n_z is the unit normal vector along the positive z-axis. The detailed expressions of F_z, μ, and λ can be found in [18].

On the basis of the motion equation in the frequency domain, the heave response amplitude ζ can be expressed as:

$$\zeta = \frac{F_z}{-\omega^2(M+\mu) - i\omega(\lambda + \lambda_{PTO}) + K} \tag{19}$$

where λ_{PTO} denotes the PTO damping. For $\lambda_{PTO} = 0$ and $\lambda_{PTO} = \infty$, free heave-motion and fixed types, can be defined respectively. The optimal PTO damping can be defined as $\lambda_{optimal} = \sqrt{(K/\omega - \omega(M+\mu))^2 + \lambda^2}$ according to [19]. Correspondingly, the heave RAO is defined as $\xi = \zeta/A$.

The incident wave power can be theoretically calculated as:

$$P_{incident} = \frac{1}{4}\frac{\rho g A^2 \omega}{k}\left(1 + \frac{2h_1 k}{\sinh 2h_1 k}\right) \tag{20}$$

The absorbed power of the device with the PTO damping λ_{PTO} can be written as (see [19]):

$$P_{capture} = \frac{1}{2}\lambda_{PTO}\omega^2 \frac{|F_z|^2}{(K - \omega^2(M+\mu))^2 + (\omega(\lambda_{PTO} + \lambda))^2} \tag{21}$$

The CWR η is an important indicator to evaluate the hydrodynamic efficiency of WECs and can be calculated as $\eta = P_{capture}/P_{incident}$.

As indicators of breakwater performance, the reflection coefficient K_r and transmission coefficient K_t can be written as:

$$K_t = \left| \frac{\Phi_I + \Phi_D - i\omega\zeta\varphi_R}{\Phi_I} \right|_{x=+\infty} \tag{22}$$

$$K_r = \left| \frac{\Phi_D - i\omega\zeta\varphi_R}{\Phi_I} \right|_{x=-\infty} \tag{23}$$

3. Dimensional Analysis

The dimensional parameters include wavenumber k, water density ρ, gravitational acceleration g, water depth h_1, incident wave amplitude A, breadth B, draft d_1, PTO damping λ_{PTO} and heave response amplitude in heave ζ. The objective parameter includes the outputted power $P_{capture}$, reflected wave amplitude A_r and transmitted wave amplitude A_t. The incident wave amplitude, water depth, water density and gravitational acceleration are fixed parameters in this analysis. P_{ref} denotes an arbitrary reference power level and λ_{ref} an arbitrary reference damping level. According to the Buckingham's theorem [20], the dimensionless variables can be determined (details see Table 1). Here, the incident wave power (i.e., $P_{incident}$) was chosen as P_{ref} and the optimal PTO damping $\lambda_{optimal}$ as λ_{ref} [21]. Thus, the dimensionless outputted power can be expressed as the CWR η (=$P_{capture}/P_{incident}$). The reflected wave and the transmitted wave are dimensionalized by the incident wave amplitude A. Correspondingly, the dimensionless reflected wave and transmitted wave can be expressed as the reflection coefficient K_r (=A_r/A) and the transmission coefficient K_t (=A_t/A). Then, we can write the CWR, reflection coefficient and transmission coefficient as function of the dimensionless wavenumber kh_1, relative breadth B/h_1, relative draft d_1/h_1 and relative PTO damping $\lambda_{PTO}/\lambda_{optimal}$.

$$\begin{aligned} \eta &= f\left(B/h_1,\, d_1/h_1,\, kh_1,\, \lambda_{PTO}/\lambda_{optimal}\right) \\ K_r &= f\left(B/h_1,\, d_1/h_1,\, kh_1,\, \lambda_{PTO}/\lambda_{optimal}\right) \\ K_t &= f\left(B/h_1,\, d_1/h_1,\, kh_1,\, \lambda_{PTO}/\lambda_{optimal}\right) \end{aligned} \tag{24}$$

Table 1. Outline of dimensional analysis.

Dimensional Variables	Physical Unit	Nondimensional Variables
Water density, ρ	$kg{\cdot}m^{-3}$	-
Gravitational acceleration, g	$m{\cdot}s^{-2}$	-
Water depth, h_1	m	-
Incident wave amplitude, A	m	-
Wavenumber, k	m^{-1}	$\pi_1 = kh_1$
Breadth, B	m	$\pi_2 = B/h_1$
Draft, d_1	m	$\pi_3 = d_1/h_1$
PTO damping, λ_{PTO}	$kg{\cdot}s^{-1}$	$\pi_4 = \lambda_{PTO}/\lambda_{ref}$
Response amplitude in heave, ζ	m	$\pi_5 = \zeta/A$
Outputted power, $P_{capture}$	$kg{\cdot}m^2{\cdot}s^{-3}$	$\pi_a = P_{capture}/P_{ref}$
Reflected wave amplitude, A_r	m	$\pi_b = A_r/A$
Transmitted wave amplitude, A_t,	m	$\pi_c = A_t/A$

4. Results and Discussion

4.1. Validation

First, the correctness of the present formulation for the reflection coefficient K_r and transmission coefficient K_t is considered. Figure 2 shows the variations of K_r and K_t with the dimensionless wavenumber kh_1 obtained by the present analytical model and the corresponding numerical results [22]. The geometrical parameters are $a = h_1$, $d_1 = 0.5h_1$, and h_1 =1 m; $\lambda_{PTO} = 10000\ \lambda_{optimal}$ is used to solve

for the motion equation in the present study, in order to have the pontoon fixed as in [22]. The incident wave amplitude is A = 0.1 m. The maximum difference between the present and reference results for the reflection and transmission coefficients are 5% and 2.5%, respectively. As shown, a good agreement can be achieved.

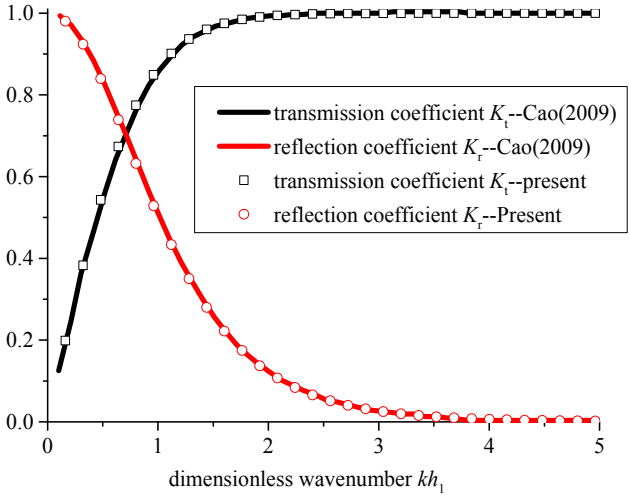

Figure 2. Comparison of transmission coefficient K_r and reflection coefficient K_t obtained by the present approach with the results of [22].

The accuracy of the heave RAO ξ is then verified against the numerical results obtained by Isaacson et al. [23] for $B = 3d_1$ and $d_1 = 0.2h_1$. Since the breakwater is constrained to heave motion, but no PTO damping was considered in [23], the value chosen for the PTO damping λ_{PTO} is 0 in the present study. Figure 3 shows the comparison of the heave RAO obtained using the present approach with the results obtained in [23].The maximum difference between the present and reference results for the heave RAO is 4.5%. It can be seen that a good agreement can be obtained.

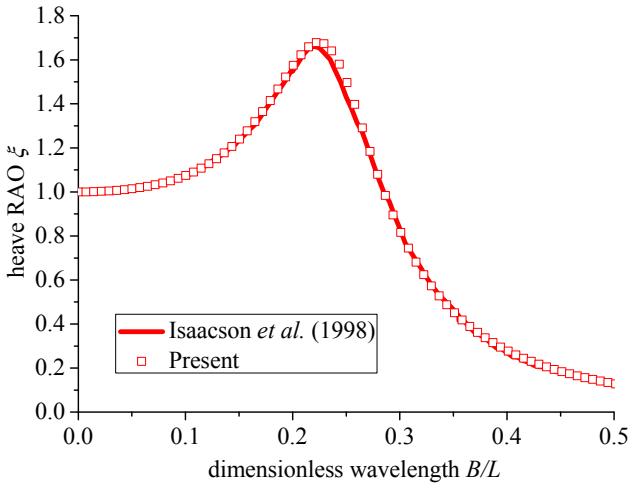

Figure 3. Comparison of the heave response amplitude operator (RAO) obtained using the present approach with the results of Isaacson et al. [23]. (B/L represents the dimensionless wavelength).

Lastly, the CWR η is verified by using the relation of $K_t^2 + K_r^2 + \eta = 1$ [24]. The detailed validation is described in Figure 4. As shown, the aforementioned condition is accurately satisfied.

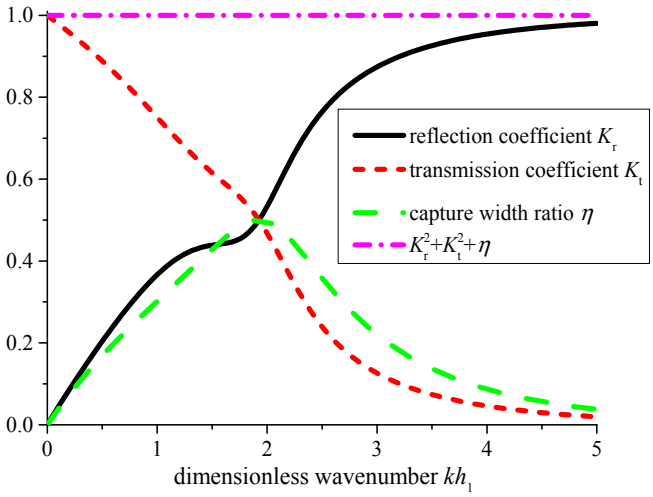

Figure 4. Variations of the reflection coefficient K_r, transmission coefficient K_t, capture width ratio (CWR) η, and $K_t^2 + K_r^2 + \eta$ with the dimensionless wavenumber kh_1 for the breakwater with the optimal PTO damping.

4.2. Comparison of the Different Breakwater Systems

From the standpoint of the WEC, the optimal PTO damping is often used to assess the performance of the devices. In the Sections 4.2–4.4 the relationships between the reflection coefficient K_r, transmission coefficient K_t, and CWR η for the proposed integrated device with the optimal PTO damping $\lambda_{optimal}$ are critical in determining the frequency region in which the acceptable wave attenuation performance and the efficient wave energy conversion can be obtained.

To illustrate the features of the integrated system with the optimal PTO damping, the hydrodynamic performance corresponding to the breakwater with the optimal PTO damping (case 1), free heave-motion breakwater (case 2), and fixed breakwater (case 3) are compared. The geometrical parameters are d_1 = 2.5 m, B = 8 m, and h_1 = 10 m (i.e., B/h_1 = 0.8 and d_1/h_1 = 0.25). The incident wave amplitude is A = 1.0 m. Figures 4–6 present a comparison of the three cases with respect to the reflection coefficient K_r, transmission coefficient K_t, and heave RAO ξ, respectively.

As shown in Figure 5, the reflection coefficient of fixed breakwater is larger than those of the others. Figure 6 shows that the transmission coefficient of the breakwater with the optimal PTO damping is near to that of the fixed breakwater; they are markedly smaller than that of the free heave-motion breakwater. The heave RAO of the fixed breakwater is null; thus, it is not plotted in Figure 7. As intuitively expected, the heave RAO of the PTO damping-controlled breakwater is markedly smaller than that of the free heave-motion breakwater, which may be beneficial to improve the stability of the breakwater. By introducing the PTO damping, the breakwater performance can be improved significantly and the heave RAO can be reduced.

Figure 4 shows the variations of K_t, K_r, η, and $K_t^2 + K_r^2 + \eta$ with the dimensionless wavenumber kh_1 for the breakwater with the optimal PTO damping. The curve of η exhibits a parabolic trend and reaches the maximum (i.e., η_{max} = 50%) at resonance. Interestingly, there exists a cross-point for the three curves at which η is 50%, and both K_r and K_t are 0.5. This observation indicates that 25% of the incident wave energy is reflected toward the left, 25% is transmitted toward the right, and the remaining 50% is absorbed. This is a consequence of wave energy theory (see [19] (p. 198)). The condition $K_t < 0.5$ shall be satisfied for a qualified breakwater [25]. Therefore, the ideal frequency region with a lower threshold corresponding to the natural frequency is of interest for the integrated system with the optimal PTO damping. Since the study is conducted under the context of small amplitude assumption within linear potential theory neglecting viscous and nonlinear effects, the heave RAO of the device may not be totally in accordance with the corresponding experimental results. From the literature, it can be seen that the whole variation trends of the hydrodynamic coefficients

corresponding to analytical and experimental results are similar [23]. Thus, the analytical results may have directive significance for the practical engineering.

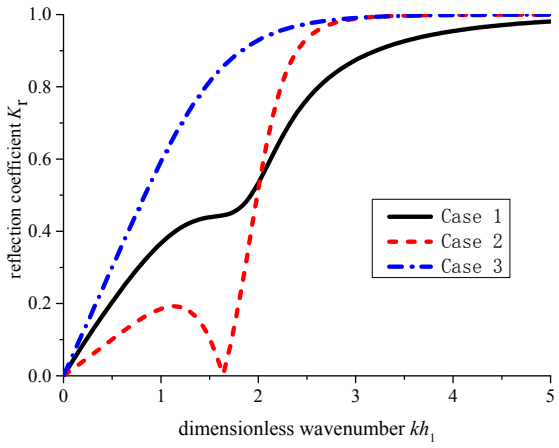

Figure 5. Variations of the reflection coefficient K_r with the dimensionless wavenumber kh_1 for cases 1–3.

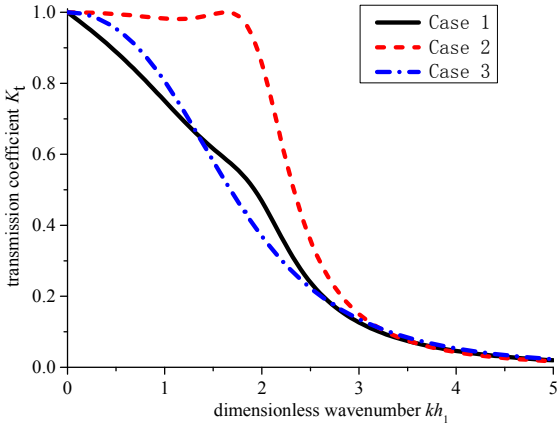

Figure 6. Variations of the transmission coefficient K_t with the dimensionless wavenumber kh_1 for cases 1–3.

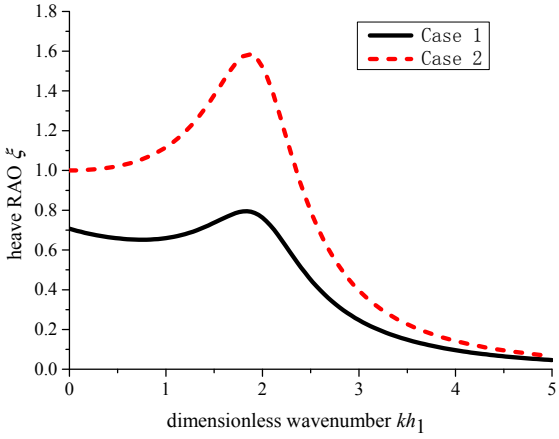

Figure 7. Variations of the heave RAO ξ with the dimensionless wavenumber kh_1 for cases 1 and 2.

4.3. Effect of the Relative Breadth B/h_1

The breadth and the draft of the pontoon are important parameters to design such a system. In Sections 4.3 and 4.4, the effects of the dimensionless breadth (i.e., relative breadth B/h_1) and dimensionless draft (i.e., relative draft d_1/h_1) on the hydrodynamic properties of the system are conducted, respectively. Figures 8–11 show the variations of the reflection coefficient K_r, transmission coefficient K_t, CWR η and heave RAO ξ with the dimensionless wavenumber kh_1 for different relative breadths B/h_1 (=0.2, 0.5, 0.8, 1.1 and 1.4). The other geometrical parameters are d_1 = 2.5 m and h_1 = 10 m (i.e., d_1/h_1 = 0.25). The incident wave amplitude A is 1.0 m. Optimal damping is used in this subsection. From Figures 8 and 9, it can be seen that, for the pontoon-type floating breakwater, the wider the breadth of the breakwater, the more effective is the wave barrier [17,25]. For the CWR, the maximum CWR does not vary with the relative draft. The maximum heave RAO obviously increases with the decreasing of the relative breadth. The dimensionless wavenumber kh_1 corresponding to the maximum heave RAO (or the CWR) decreases with the increasing of the relative breadth. It is due to the fact that the natural frequencies of the pontoon decrease with the increasing of the relative breadth.

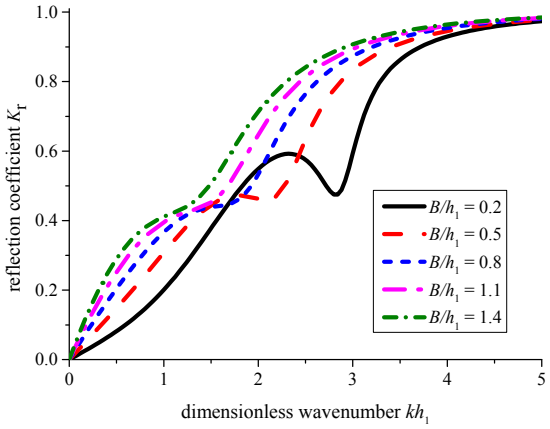

Figure 8. Variations of the reflection coefficient K_r with the dimensionless wavenumber kh_1 for cases of relative draft d_1/h_1 = 0.25 and PTO damping $\lambda_{PTO} = \lambda_{optimal}$ ($\lambda_{optimal}$ refers to the optimal PTO damping).

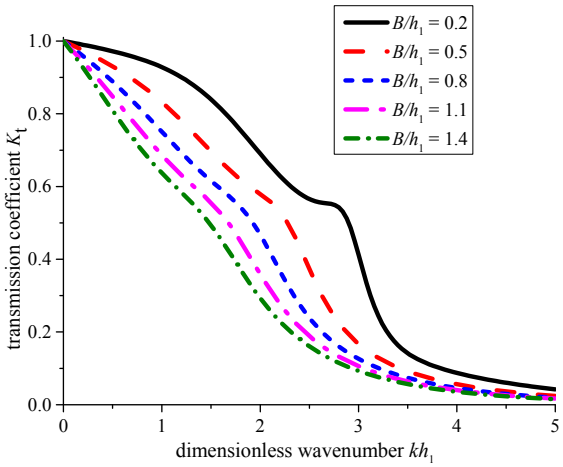

Figure 9. Variations of the transmission coefficient K_t with the dimensionless wavenumber kh_1 for cases of d_1/h_1 = 0.25 and $\lambda_{PTO} = \lambda_{optimal}$.

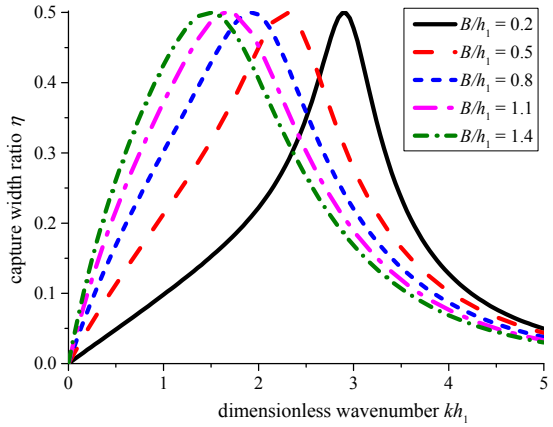

Figure 10. Variations of the CWR η with the dimensionless wavenumber kh_1 for cases of $d_1/h_1 = 0.25$ and $\lambda_{PTO} = \lambda_{optimal}$.

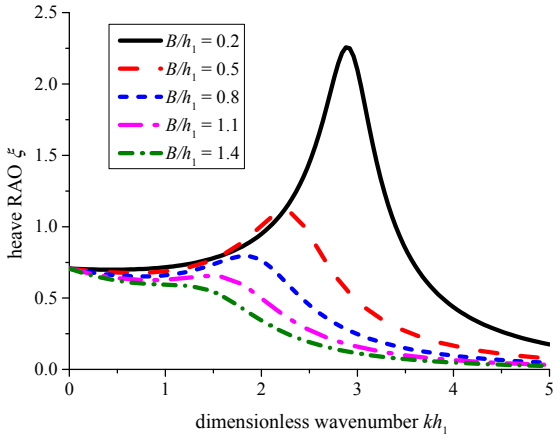

Figure 11. Variations of the heave RAO ξ with the dimensionless wavenumber kh_1 for cases of $d_1/h_1 = 0.25$ and $\lambda_{PTO} = \lambda_{optimal}$.

4.4. Effect of the Relative Draft d_1/h_1

Figures 12–15 show the variations of the reflection coefficient K_r, transmission coefficient K_t, CWR η and heave RAO ξ with the dimensionless wavenumber kh_1 for different relative drafts $d_1/h_1 = 0.05$, 0.15, 0.25, 0.35 and 0.45. The other geometrical parameters are $B = 8$ m and $h_1 = 10$ m (i.e., $B/h_1 = 0.8$). The incident wave amplitude A is 1.0 m. From Figures 12 and 13, it can be seen that, the deeper the draft of the breakwater, the more effective is the wave barrier. For the CWR, the effective frequency bandwidth ($\eta > 20\%$) narrows with an increase in the draft. However, the maximum CWR does not vary with the relative draft. The maximum heave RAO increases with the increasing of the relative draft. Note that, since the natural frequencies of the pontoon decreases with the increasing of relative draft, the kh_1 corresponding to the maximum CWR and heave RAO decreases accordingly.

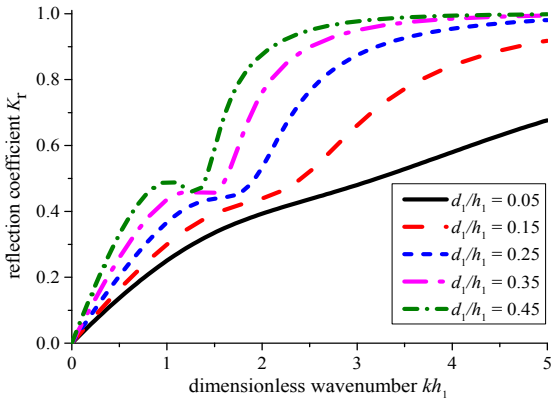

Figure 12. Variations of the reflection coefficient K_r with the dimensionless wavenumber kh_1 for cases of relative breadth $B/h_1 = 0.8$ and $\lambda_{PTO} = \lambda_{optimal}$.

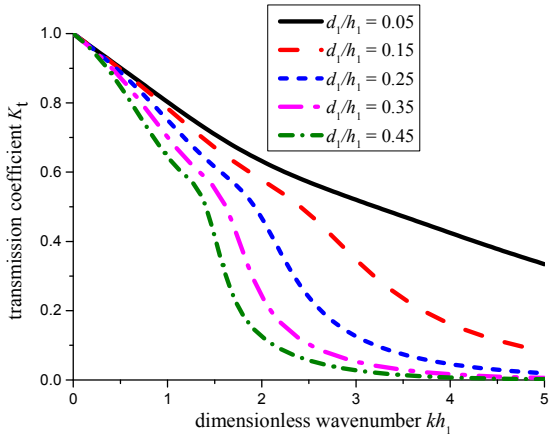

Figure 13. Variations of the transmission coefficient K_t with the dimensionless wavenumber kh_1 for cases of $B/h_1 = 0.8$ and $\lambda_{PTO} = \lambda_{optimal}$.

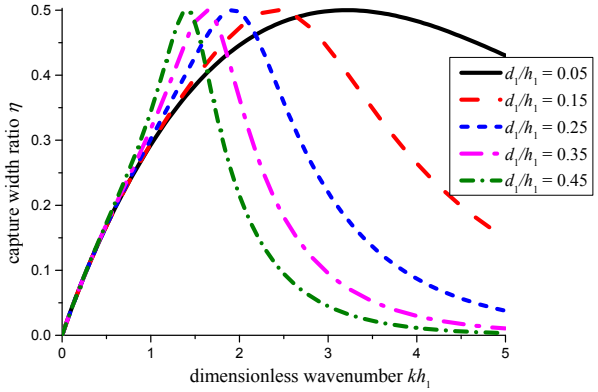

Figure 14. Variations of the CWR η with the dimensionless wavenumber kh_1 for cases of $B/h_1 = 0.8$ and $\lambda_{PTO} = \lambda_{optimal}$.

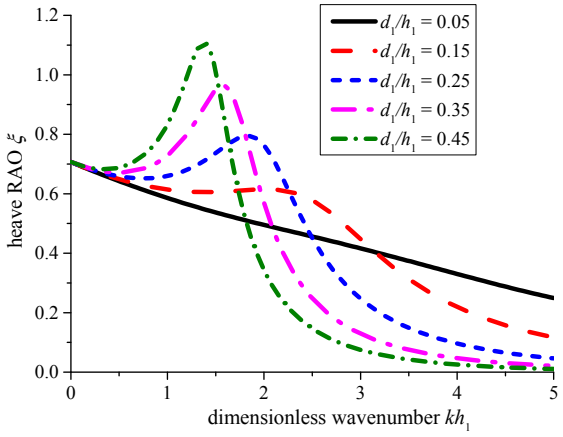

Figure 15. Variations of the heave RAO ξ with the dimensionless wavenumber kh_1 for cases of $B/h_1 = 0.8$ and $\lambda_{PTO} = \lambda_{optimal}$.

4.5. Effect of the PTO Damping

The integrated system with the optimal PTO damping, which may lead to the optimization of the CWR, is investigated in Sections 4.2–4.4. Given that both the wave attenuation performance and wave energy extraction efficiency shall be considered simultaneously for the integrated system, the effect of the PTO damping on the reflection coefficient K_r, transmission coefficient K_t, and CWR η are considered. The geometrical parameters are $d_1 = 2.5$ m, $B = 8$ m and $h_1 = 10$ m (i.e., $d_1/h_1 = 0.25$, $B/h_1 = 0.8$). The incident wave amplitude A is 1.0 m. The values selected for the tested PTO dampings are $\lambda_{PTO} = 0.8\lambda_{optimal}$, $1.0\lambda_{optimal}$, $1.5\lambda_{optimal}$, $2.0\lambda_{optimal}$, $5.0\lambda_{optimal}$, and $\lambda_{PTO} = 10000\lambda_{optimal}$ (i.e., the case of the fixed breakwater).

Figure 16 shows the variations of the reflection coefficient K_r with the dimensionless wavenumber kh_1. As observed, the reflection coefficient increases with an increase in the PTO damping. Figures 17 and 18 show the variations of the transmission coefficient and heave RAO against kh_1. With an increase in the PTO damping, the heave RAO decreases (referring to Figure 18); the transmission coefficient increases in the lower frequencies and, differently, the trend of decreasing firstly and then increasing was found in the middle frequency region (i.e., $1.3 < kh_1 < 2.7$). These findings indicate that the wave attenuation performance can be superior to the fixed breakwater by proper adjustment of the PTO damping. Figure 19 shows the variations of the CWR η with kh_1. Since the natural frequency ω_{nat} of the pontoon in heave mode can be expressed as $\omega_{nat} = \sqrt{\frac{K}{M+\mu}}$, changes in the PTO damping do not affect the natural frequency of the system [26]. Thus, the locations (i.e., kh_1) of the CWR peak value are similar for the different cases. With an increase in the PTO damping, the CWR first increases and then decreases. Notably, the CWR corresponding to the PTO damping of $\lambda_{PTO} = 1.5\lambda_{optimal}$ (or $\lambda_{PTO} = 2\lambda_{optimal}$) is only slightly inferior to the case with the optimal PTO damping in the range of $1.3 < kh_1 < 2.7$; under this condition, the transmission coefficient of the former is superior to the latter. Specifically, considering the conditions $K_t < 0.5$ and $\eta > 20\%$, the available frequency region is $1.925 < kh_1 < 3.075$ when $\lambda_{PTO} = 1\lambda_{optimal}$; $1.723 < kh_1 < 3.02$ when $\lambda_{PTO} = 1.5\lambda_{optimal}$, and $1.625 < kh_1 < 2.92$ when $\lambda_{PTO} = 2\lambda_{optimal}$. That is, the effective frequency bandwidth is broadened when $\lambda_{PTO} = 1.5$–$2\lambda_{optimal}$.

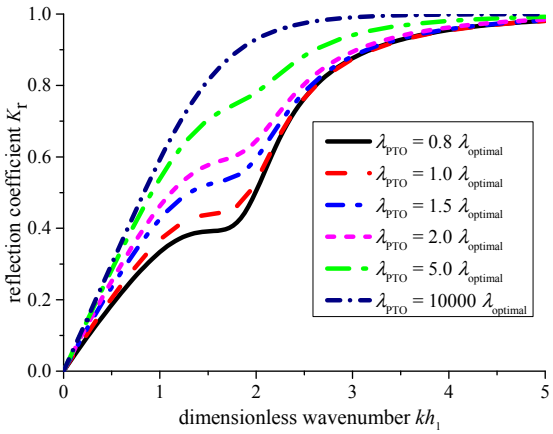

Figure 16. Variations of the reflection coefficient K_r with the dimensionless wavenumber kh_1 for cases of $d_1/h_1 = 0.25$ and $B/h_1 = 0.8$.

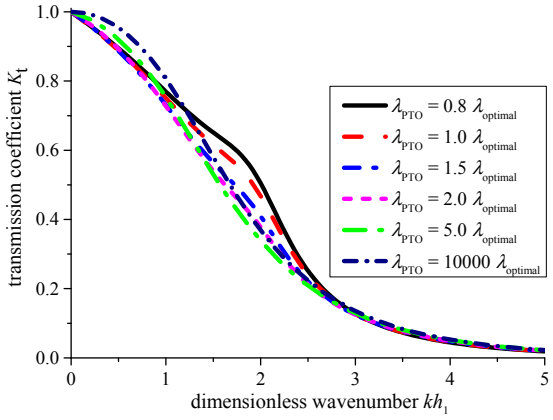

Figure 17. Variations of the transmission coefficient K_t with the dimensionless wavenumber kh_1 for cases of $d_1/h_1 = 0.25$ and $B/h_1 = 0.8$.

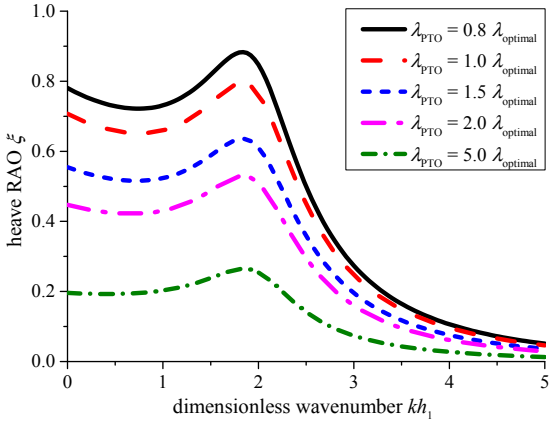

Figure 18. Variations of the heave RAO ξ with the dimensionless wavenumber kh_1 for cases of $d_1/h_1 = 0.25$ and $B/h_1 = 0.8$.

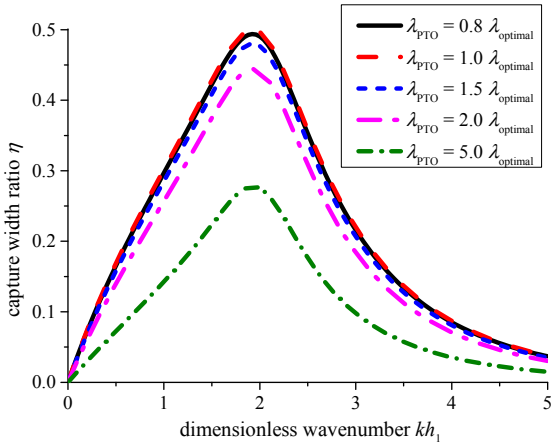

Figure 19. Variations of the CWR η with the dimensionless wavenumber kh_1 for cases of $d_1/h_1 = 0.25$ and $B/h_1 = 0.8$.

5. Conclusions

The hydrodynamic properties of a WEC-type floating breakwater system is investigated theoretically based on linear potential flow theory. The breakwater is constrained in heave motion. The linear PTO damping is used to calculate the absorbed power. The hydrodynamic properties of the breakwater with the optimal PTO damping, fixed breakwater, and free heave-motion breakwater are compared. The effect of the PTO damping on the performance of the integrated system is particularly evaluated in this study.

The following conclusions can be drawn from this study:

(1) Compared with that of the free heave-motion breakwater, the wave attenuation performance of the breakwater is improved for the proposed integrated system.

(2) For the system with the optimal PTO damping, the low threshold of the practical frequency region corresponds to the natural frequency.

(3) With a decrease in the heave RAO of the breakwater, the transmission coefficient increases in the lower-frequency region, although a decreasing trend is initially observed, followed by an increasing trend in the middle-frequency region.

(4) Due to the changing of the natural frequency, the effect of the relative breadth B/h_1 and relative draft d_1/h_1 of the pontoon affect the performance of the system significantly. This shall be paid attention while such a system is designed.

(5) The breakwater with the PTO damping of $\lambda_{PTO} = 1.5–2\lambda_{optimal}$ may give a broader frequency bandwidth with $K_t < 0.5$ and $\eta > 20\%$. Fortunately, the transmission coefficient corresponding to the case with $\lambda_{PTO} = 2\lambda_{optimal}$ is slightly superior to that of the fixed breakwater.

(6) The proposed system is theoretically proved to produce power effectively and, at the same time, the function of coastal protection can be comparable to that of the fixed breakwater.

From the point of engineering application, the proposed scheme is more applicable for the pile-restrained floating breakwater, for which the pontoon moves in heave motion under the control of the vertical pile [17,23]. Heave-type floating bodies are often used to capture wave energy [24]. Thus, the effects of the non-heave motions are not considered. This preliminary investigation is performed under frame of linear potential theory in frequency domain. The linear damping is adopted to calculate the produced power and conduct the parametric study. In practice, the nonlinear PTO damping (such as Coulomb damping) is often used for the hydraulic PTO system [27]. Despite this, the theoretical results predict the potential application. We can design the breakwater system based on the sea state (such as dominating wave length L) at the deployment site. It is well understood that the disadvantage

of the pontoon type breakwater is the bad breakwater performance in long waves [23]. In the future research, we will focus on how to improve the wave attenuation performance of the proposed system.

Acknowledgments: This work was financially supported by the National Natural Science Foundation of China (Grant Nos. 51679036, 51490672 and 51379037) and Royal Academy of Engineering under the UK-China Industry Academia Partnership Programme (Grant No.UK-CIAPP\73).

Author Contributions: Xuanlie Zhao, Dezhi Ning, Chongwei Zhang and Haigui Kang draft the work, make substantial contributions to the design of the work, make final approval of the version to be published and make agreement to be accountable for all aspects of the work in ensuring that questions related to the accuracy or integrity of any part of the work are appropriately investigated and resolved.

Conflicts of Interest: The authors declare no conflict of interest.

References

1. You, Y.G.; Zheng, Y.H.; Shen, Y.M.; Wu, B.J.; Liu, R. Wave energy study in China: Advancements and perspectives. *China Ocean Eng.* **2003**, *17*, 101–109.
2. Falcão, A.F.d.O. Wave energy utilization: A review of the technologies. *Renew. Sustain. Energy Rev.* **2010**, *14*, 899–918. [CrossRef]
3. Ferro, B.D. Wave and tidal energy: Its emergence and the challenges it faces. *Refocus* **2006**, *7*, 46–48. [CrossRef]
4. Lirn, T.C.; Wu, Y.C. J.; Chen, Y.J. Green performance criteria for sustainable ports in Asia. *Int. J. Phys. Distrib. Logist. Manag.* **2013**, *43*, 427–451. [CrossRef]
5. Park, J.Y.; Yeo, G.T. An Evaluation of Greenness of major Korean ports: A Fuzzy Set Approach. *Asian J. Shipp. Logist.* **2012**, *28*, 67–82. [CrossRef]
6. Mustapa, M.A.; Yaakob, O.B.; Ahmed, Y.M.; Rheem, C.; Koh, K.K.; Adnan, F.A. Wave energy device and breakwater integration: A review. *Renew. Sustain. Energy Rev.* **2017**, *77*, 43–58. [CrossRef]
7. Contestabile, P.; Iuppa, C.; Lauro, E.D.; Cavallaro, L.; Andersen, T.L.; Vicinanza, D. Wave loadings acting on innovative rubble mound breakwater for overtopping wave energy conversion. *Coast. Eng.* **2017**, *122*, 60–74. [CrossRef]
8. Iuppa, C.; Contestabile, P.; Cavallaro, L.; Foti, E.; Vicinanza, D. Hydraulic Performance of an Innovative Breakwater for Overtopping Wave Energy Conversion. *Sustainability* **2016**, *8*, 1226. [CrossRef]
9. Takahashi, S.; Nakada, H.; Ohneda, H.; Shikamori, M. Wave power conversion by a prototype wave power extracting caisson in Sakata port. *Coast. Eng. Proc.* **1991**, *1*, 3440–3453.
10. Arena, F.; Romolo, A.; Malara, G.; Ascanelli, A. On design and building of a U-OWC wave energy converter in the Mediterranean Sea: A case study. In Proceedings of the 32nd International Conference on Ocean, Offshore and Arctic Engineering, Nantes, France, 9–14 June 2013.
11. Yueh, C.Y.; Chuang, S.H. A boundary element model for a partially piston-type porous wave energy converter in gravity waves. *Eng. Anal. Bound. Elements* **2012**, *36*, 658–664. [CrossRef]
12. McCartney, B.L. Floating breakwater design. *J. Waterw. Port Coast. Ocean Eng.* **1985**, *111*, 304–318. [CrossRef]
13. He, F.; Huang, Z.H.; Law, W.K. An experimental study of a floating breakwater with asymmetric pneumatic chambers for wave energy extraction. *Appl. Energy* **2013**, *106*, 222–231. [CrossRef]
14. Mendoza, E.; Silva, R.; Zanuttigh, B.; Angelelli, E.; Lykke Andersen, T.; Martinelli, L.; Ruol, P. Beach response to wave energy converter farms acting as coastal defense. *Coast. Eng.* **2014**, *87*, 97–111. [CrossRef]
15. Chen, B.; Ning, D.Z.; Liu, C.Q.; Greated, C.A.; Kang, H.G. Wave energy extraction by horizontal floating cylinders perpendicular to wave propagation. *Ocean Eng.* **2016**, *121*, 112–122. [CrossRef]
16. Martinelli, L.; Ruol, P.; Favaretto, C. Hybrid structure combining a wave energy converter and a floating breakwater. In Proceedings of the International Offshore and Polar Engineering Conference, Rhodes, Greece, 26 June–2 July 2016.
17. Ning, D.Z.; Zhao, X.L.; Göteman, M.; Kang, H.G. Hydrodynamic performance of a pile-restrained WEC-type floating breakwater: An experimental study. *Renew. Energy* **2016**, *95*, 531–541. [CrossRef]
18. Zheng, Y.H.; You, Y.G.; Shen, Y.M. On the radiation and diffraction of water waves by a rectangular buoy. *Ocean Eng.* **2004**, *31*, 1063–1082. [CrossRef]
19. Falnes, J. *Ocean Waves and Oscillating Systems*; Cambridge University Press: Cambridge, UK, 2002.
20. Sonin, A.A. *The Physical Basis of Dimensional Analysis*, 2nd ed.; MIT Department of Mechanical Engineering: Cambridge, MA, USA, 2001.

21. Bódai, T.; Srinil, N. Performance analysis and optimization of a box-hull wave energy converter concept. *Renew. Energy* **2015**, *81*, 551–565. [CrossRef]
22. Cao, F.S. The application of scaled boundary finite element method in potential flow theory. Ph.D. Thesis, Dalian University of Technology, Dalian, China, 2009.
23. Isaacson, M.; Baldwin, J.; Bhat, S. Wave propagation past a pile-restrained floating breakwater. *Int. J. Offshore Polar Eng.* **1998**, *8*, 265–269.
24. Mei, C.C. Hydrodynamic principles of wave power extraction. *Philos. Trans. R. Soc. A-Math. Phys. Eng. Sci.* **2012**, *370*, 208–234. [CrossRef] [PubMed]
25. Koutandos, E.; Prinos, P.; Gironella, X. Floating breakwaters under regular and irregular wave forcing: Reflection and transmission characteristics. *J. Hydraul. Res.* **2005**, *43*, 174–188. [CrossRef]
26. Cheng, Z.S.; Yang, J.M.; Hu, Z.Q.; Xiao, L.F. Frequency/time domain modeling of a direct drive point absorber wave energy converter. *Sci. China Phys. Mech. Astron.* **2014**, *57*, 311–320. [CrossRef]
27. Babarit, A.; Halsb, J.; Muliawan, M.J.; Kurniawan, A.; Moan, T.; Krokstad, J. Numerical benchmarking study of a selection of wave energy converters. *Renew. Energy* **2012**, *41*, 44–63. [CrossRef]